The Arf GAP SMAP2 is necessary for organized vesicle budding from the *trans*-Golgi network and subsequent acrosome formation in spermiogenesis

Tomo Funaki[a,*], Shunsuke Kon[a,*], Kenji Tanabe[b], Waka Natsume[a], Sayaka Sato[a], Tadafumi Shimizu[a], Naomi Yoshida[a], Won Fen Wong[a], Atsuo Ogura[c], Takehiko Ogawa[d], Kimiko Inoue[c], Narumi Ogonuki[c], Hiromi Miki[c], Keiji Mochida[c], Keisuke Endoh[c], Kentarou Yomogida[e], Manabu Fukumoto[a], Reiko Horai[f], Yoichiro Iwakura[f], Chizuru Ito[g], Kiyotaka Toshimori[g], Toshio Watanabe[h], and Masanobu Satake[a]

[a]Department of Molecular Immunology, Department of Pathology, Institute of Development, Aging and Cancer, Tohoku University, Sendai 980-8575, Japan; [b]Medical Research Institute, Tokyo Women's Medical University, Tokyo 162-8666, Japan; [c]RIKEN Bio Resource Center, Tsukuba 305-0074, Japan; [d]Department of Urology, Yokohama City University Graduate School of Medicine, Yokohama 236-0004, Japan; [e]Department of Food Science and Nutrition, School of Human Environmental Science, Mukogawa Women's University, Nishinomiya 663-8558, Japan; [f]Institute of Medical Science, University of Tokyo, Tokyo 108-8639, Japan; [g]Department of Anatomy and Developmental Biology, Chiba University Graduate School of Medicine, Inohana 260-8670, Japan; [h]Department of Biological Sciences, Nara Women's University, Nara 630-8506, Japan

ABSTRACT **The *trans*-Golgi network (TGN) functions as a hub organelle in the exocytosis of clathrin-coated membrane vesicles, and SMAP2 is an Arf GTPase-activating protein that binds to both clathrin and the clathrin assembly protein (CALM). In the present study, SMAP2 is detected on the TGN in the pachytene spermatocyte to the round spermatid stages of spermatogenesis. Gene targeting reveals that *SMAP2*-deficient male mice are healthy and survive to adulthood but are infertile and exhibit globozoospermia. In *SMAP2*-deficient spermatids, the diameter of proacrosomal vesicles budding from TGN increases, TGN structures are distorted, acrosome formation is severely impaired, and reorganization of the nucleus does not proceed properly. CALM functions to regulate vesicle sizes, and this study shows that CALM is not recruited to the TGN in the absence of SMAP2. Furthermore, syntaxin2, a component of the soluble *N*-ethylmaleimide–sensitive factor attachment protein receptor (SNARE) complex, is not properly concentrated at the site of acrosome formation. Thus this study reveals a link between SMAP2 and CALM/syntaxin2 in clathrin-coated vesicle formation from the TGN and subsequent acrosome formation. *SMAP2*-deficient mice provide a model for globozoospermia in humans.**

Monitoring Editor
Julie Brill
The Hospital for Sick Children

Received: May 3, 2013
Revised: Jun 14, 2013
Accepted: Jul 1, 2013

This article was published online ahead of print in MBoC in Press (http://www.molbiolcell.org/cgi/doi/10.1091/mbc.E13-05-0234) on July 17, 2013.

*These authors contributed equally to this work.

The authors have no conflicting financial interests.

Address correspondence to: Masanobu Satake (satake@idac.tohoku.ac.jp).

Abbreviations used: Arf GAP, Arf GTPase-activating protein; CALM, clathrin assembly protein; DAPI, 4′,6-diamidino-2-phenylindole; DIC, differential interference contrast; GEF, guanine nucleotide exchanging factor; PAS, periodic acid-Schiff stain; PBS, phosphate-buffered saline; PNA, peanut agglutinin; SNARE, soluble *N*-ethylmaleimide–sensitive factor attachment protein receptor; TEM, transmission electron microscopy; TGN, *trans*-Golgi network; VAMP, vesicle-associated membrane proteins.

INTRODUCTION

The cells of all eukaryotic organisms possess a trafficking system of membrane vesicles that is vital to maintaining cellular homeostasis. It was suggested that the dysregulation of this trafficking is involved in the genesis of tumors as well as in neurodegenerative diseases in humans (McMahon and Boucrot, 2011). As a caveat, in most cases, this hypothesis merely reflects the fact that the gene discovered in one study as responsible for disease onset or progression is known from another study to be involved in vesicle trafficking. Therefore it is not always clear how the possible dysregulation of vesicle trafficking inside the cells might lead to the pathologies seen in particular diseases. One of the reasons for this lack of knowledge is the relatively scant number of studies targeting genes involved in vesicle trafficking.

Clathrin-coated vesicles represent one type of membrane vesicle and are used in a broad range of trafficking pathways, including endocytosis and exocytosis of membrane proteins. The formation of clathrin-coated vesicles is regulated in a coordinated manner by many molecules and Arf proteins, which belong to a family of small GTPases and play key roles in the process (D'Souza-Schorey and Chavrier, 2006; Gillingham and Munro, 2007; Kahn, 2009; Donaldson and Jackson, 2011). The GTPase activity of Arf is activated by an Arf GTPase-activating protein (Arf GAP). Of interest, Arf GAP not only functions as a GAP for Arf but also possesses an Arf-independent function that contributes to the formation of clathrin-coated vesicles (Randazzo and Hirsch, 2004; Spang *et al.*, 2010; Kahn, 2011; Kon *et al.*, 2011).

There are 31 Arf GAP family proteins, and SMAP1 and SMAP2 constitute a small subgroup. SMAPs harbor a clathrin-binding motif and a domain capable of binding to the clathrin assembly protein (CALM; Tanabe *et al.*, 2005, 2006; Natsume *et al.*, 2006). Because of these characteristics, SMAP may exert unique functions in the formation of clathrin-coated vesicles that are not seen in the other Arf GAPs. For example, SMAP1 functions as an Arf6-specific GAP in the endocytosis of the transferrin receptor and is also involved in sorting of endocytosed c-Kit from multivesicular bodies to lysosomes (Tanabe *et al.*, 2005; Kon *et al.*, 2008, 2013). SMAP2 exhibits a similar extent of GAP activity for both Arf1 and Arf6 in vitro. SMAP2 most likely behaves as an Arf1-preferring GAP in cells, however, since the introduction of a GAP-negative mutant of SMAP2 renders cells resistant to brefeldin A, an inhibitor of Arf1 guanine nucleotide exchanging factor (GEF) but not Arf6 GEF (Natsume *et al.*, 2006). Moreover, SMAP2 is localized on early endosomes and the *trans*-Golgi network (TGN) and appears to function in the early endosome–to-TGN transport of TGN46/38 and in the TGN-to–plasma membrane transport of the vesicular stomatitis virus G protein (Natsume *et al.*, 2006; Funaki *et al.*, 2011). Furthermore, SMAP2 can compensate for the lack of SMAP1 in endocytosis of the transferrin receptor (Kon *et al.*, 2013). Therefore SMAP2 may play multiple roles in various intracellular trafficking pathways.

All of the foregoing findings regarding SMAP1 and SMAP2 were obtained using cell cultures in vitro (Tanabe *et al.*, 2005; Natsume *et al.*, 2006; Kon *et al.*, 2008; Funaki *et al.*, 2011). Recently we reported that *SMAP1*-targeted cells have defects in the trafficking of the transferrin receptor as well as c-Kit, and targeted mice are predisposed to develop myelodysplastic syndrome and, eventually, acute myeloid leukemia (Kon *et al.*, 2013). These results demonstrate a possible link between the dysregulated endocytosis in cells and oncogenesis. The TGN functions as a hub organelle in exocytosis by sorting either secreted molecules to the cell membrane or hydrolytic enzymes to lysosomes (Bonifacino and Rojas, 2006). How the functions of tissues/organs would be impaired if the TGN machinery is disrupted is unclear. In this study, to examine the physiological roles of SMAP2 in vivo with respect to TGN transport, we targeted *SMAP2* and found that *SMAP2*-deficient male mice were infertile and exhibited globozoospermia. Vesicle budding from the TGN, as well as acrosome formation, was disorganized in *SMAP2*-deficient spermatogenesis.

RESULTS

Generation of *SMAP2*-deficient mice

We generated *SMAP2*-deficient mice using a gene-targeting method. A *SMAP2*-targeting construct was designed to replace the Met^{init}-containing exon 1 of *SMAP2* with *LacZ* and neomycin-resistance (neo^r) gene sequences (Figure 1A). Homologous recombination should give rise to a protein consisting of the amino-terminal 12 amino acids of SMAP2 fused in-frame with *LacZ*. We obtained two independent founder mice possessing the germline-transmitted, targeted *SMAP2* allele. Because essentially similar results were obtained for both lines of mice, representative results from one of the lines are described here. To generate *SMAP2*(–/–) mice, *SMAP2*(+/–) F1 mice were mated, and the F2 offspring were genotyped by Southern blot and PCR analysis (Figure 1B). *SMAP2*(+/–) and (–/–) mice were present in the expected Mendelian ratios.

SMAP2 expression was examined in tissues of wild-type mice by Northern blot analyses (Figure 1C). Two transcripts, 2.9 and 1.3 kb, which contain the same open reading frame but differ in their 3′-untranslated regions, were detected in the tissues examined (Figure 1C, top). Because the major phenotype of *SMAP2*(–/–) mice was defective spermatogenesis, as described later, *SMAP2* expression at various stages of spermatogenesis was examined using wild-type testicular cells. *SMAP2* transcripts were detected in pachytene spermatocytes to the round spermatid stages (Figure 1C, bottom). Immunoblot analyses using lysates from brain and testis detected SMAP2 at 47 kDa in the wild-type tissue but not in the *SMAP2*(–/–) tissue (Figure 1D). This result verified the SMAP2 deficiency in the *SMAP2*-targeted mice.

Infertility and globozoospermia seen in *SMAP2*-targeted male mice

SMAP2(–/–) mice grew to adulthood and were apparently healthy, but mating outcomes were not normal. When we conducted cross-breeding experiments using *SMAP2*(–/–) mice (Table 1), we found that female *SMAP2*(–/–) mice were fertile when mated to *SMAP2*(+/–) male mice. Male *SMAP2*(–/–) mice, however, were infertile regardless of the *SMAP2* genotype of the female. Thus male infertility was detected as a phenotype of *SMAP2*-targeted mice.

Epididymides of *SMAP2*(–/–) male mice were examined, and the numbers of sperm present in the epididymides were similar in *SMAP2*(+/–) and (–/–) mice (Table 2). When epididymal sperm were observed by differential interference contrast (DIC) microscopy (Figure 2A), however, a normal hook-shaped head was observed for the *SMAP2*(+/+) sperm, whereas a cylindrical or round head was observed for the *SMAP2*(–/–) sperm. The percentages of sperm possessing hook-shaped and round heads were quantified (Table 2). A majority of *SMAP2*(+/–) sperm possessed the hook-shaped head (94%), whereas most *SMAP2*(–/–) sperm were round headed (79%). Thus the morphology of *SMAP2*(–/–) sperm is typical of globozoospermia (Dam *et al.*, 2007).

Testes were sectioned, stained with hematoxylin–eosin, and examined by light microscopy (Figure 2B). In the seminiferous tubules of *SMAP2*(+/+) testes, many elongated spermatids possessing hook-shaped heads were detected. By contrast, most spermatids in the seminiferous tubules from *SMAP2*(–/–) testes possessed round heads. Similar observations were obtained for epididymal sperm

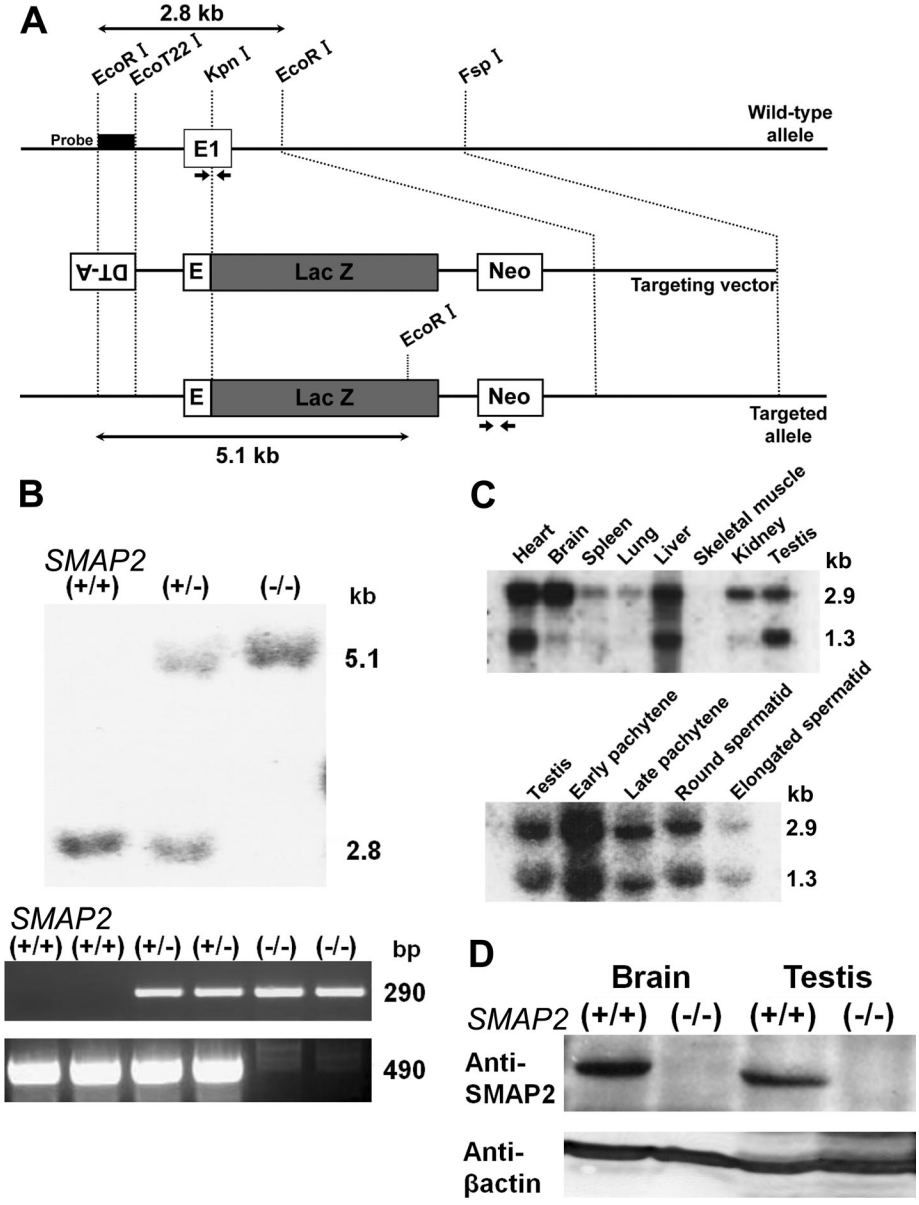

FIGURE 1: Targeting and expression of SMAP2. (A) Schematic diagram of the *SMAP2* gene. The 3′-terminal half of exon 1 in the wild-type allele was replaced by the LacZ gene in the targeted allele. Neo represents the neomycin-resistance gene used as a positive selection marker, and DT-A represents the diphtheria toxin A subunit gene. The probe for Southern blot analysis and the PCR primers used for genotyping are indicated by the rectangle and arrows, respectively. (B) Southern blot (top) and PCR (bottom) analyses of genomic DNAs that were prepared from *SMAP2*(+/+), (+/–), and (–/–) mouse tail snips. For the Southern blot, DNA was digested by *Eco*RI and hybridized by the probe shown in A. For PCR, 290– and 490–base pair bands were amplified from the targeted and wild-type alleles, respectively. (C) Northern blot analysis of RNA prepared from the indicated tissues of wild-type mice (top). Bottom, germ cells from the testes were fractionated into the indicated stages and their RNA processed for Northern blot analysis. The 2.9- and 1.3-kb bands represent *SMAP2* transcripts. (D) Immunoblot analysis of SMAP2. Protein lysates were prepared from brain and testis of *SMAP2*(+/+) and (–/–) mice and immunoblotted with an anti-SMAP2 antibody. β-Actin was used as a loading control.

(Figure 2C). Therefore the globozoospermia seen in epididymal sperm was most likely due to defects in spermatogenesis.

In humans, globozoospermia is characterized by abnormal alignment of mitochondria along the axoneme and malformation and/or lack of an acrosome (Suzuki-Toyota *et al.*, 2004). The distribution pattern of mitochondria in sperm was examined by staining cells with MitoRed (Figure 2D). In wild-type sperm, mitochondria were aligned along the axoneme, whereas in *SMAP2*-deficient sperm, some mitochondria had not moved to the axoneme but remained near the nucleus. Moreover, localization of sp56, a marker for acrosome formation, was very irregular or absent in *SMAP2*(–/–) sperm (Figure 2D). Thus the morphology of *SMAP2*(–/–) sperm indeed corresponds to globozoospermia in humans.

In mouse sperm, energy necessary for sperm motility is supplied from mitochondrial respiration according to some reports (Narisawa *et al.*, 2002; Ford, 2006) or from anaerobic glycolysis according to others (Miki *et al.*, 2004; Mukai and Okuno, 2004; Mukai and Travis, 2012). Structural changes in the mid piece, which contains the mitochondria, are closely associated with sperm motility (Wilton *et al.*, 1992; Mundy *et al.*, 1995; Piomboni *et al.*, 2012). In addition to proper motility, the acrosome reaction is also required for successful fertilization. With this background in mind, we examined the motility and fertilizing capacity of *SMAP2*(–/–) sperm in vitro. Measurements of various motility parameters revealed that the motility of *SMAP2*(–/–) sperm was significantly ($p < 0.05$) reduced compared with that of *SMAP2*(+/–) sperm (Supplemental Table S1). The decreases included percentage of motile sperm, average path velocity, straight-line velocity, curvilinear velocity, amplitude of lateral head displacement, and beat frequency. In vitro fertilization by *SMAP2*(–/–) sperm was evaluated using wild-type oocytes (Supplemental Table S2). The percentage of two-cell embryos derived from *SMAP2*(–/–) sperm was 3.9%, whereas the fertilization rate by *SMAP2*(+/–) sperm was 38%. When intracytoplasmic sperm injection experiments were performed (Supplemental Table S3), however, pups were produced at similar levels by the *SMAP2*(–/–) and (+/–) sperm (59 and 58%, respectively). Taken together, these results indicate that *SMAP2*(–/–) sperm possess a developmentally competent haploid genome but are defective in motility and ability to penetrate the oocyte.

Globozoospermia is intrinsic to *SMAP2*-targeted germ cells

SMAP2 transcripts were detected by Northern blot analyses in testes of *Sl/Sld* mice devoid of germ cells (data not shown). Because interactions between germ cells and somatic supporting cells are necessary for proper spermatogenesis, the impaired head formation in *SMAP2*(–/–) sperm could be caused by defects in the supporting cells. To examine this possibility, we conducted spermatogonial stem cell transplantations. Germ stem cells were prepared from *SMAP2*(–/–) testes

SMAP2 genotype		Number of mating trial	Average number of litters per mating
Male	Female		
(–/–)	(–/–)	4	0
(–/–)	(+/+)	11	0
(+/–)	(–/–)	4	4
(+/+)	(+/+)	4	4

TABLE 1: *SMAP2* genotype and fertility.

and injected into the seminiferous tubules of testes of W/W^v mice that lack germ cells. Three months later, differentiated spermatids were readily detected, but most exhibited the same defective round heads (Supplemental Figure S1, left). In a reciprocal transplantation experiment, germ stem cells were prepared from the testes of pCXN-EGFP transgenic mice and implanted into the seminiferous tubules of busulfan-treated *SMAP2*(–/–) animals whose testes lack germ cells. Spermatids from these transplantations possessed hook-shaped heads and appeared properly differentiated (Supplemental Figure S1, right). These results suggest that the defects causing globozoospermia are likely intrinsic to the *SMAP2*-targeted germ cells and not the supporting cells.

Stage-dependent expression and localization of SMAP2 at the TGN during spermatogenesis

SMAP2 expression during spermatogenesis was examined by immunofluorescence using a testicular cell suspension that was spun down onto microscope slides (Figure 3A). 4′,6-Diamidino-2-phenylindole (DAPI) staining showed the nuclear morphology, as well as chromatin condensation, whereas γH2AX staining detected sites of DNA double-strand breaks. Combined use of DAPI and γH2AX allowed the identification of the stages of spermatogenesis (Xu, 2003; Figure 3A). SMAP2 expression was not detected in spermatogonia or in leptotene spermatocytes but could first be detected in the cytoplasm of zygotene spermatocytes as multiple punctae. In pachytene spermatocytes and round spermatids, SMAP2 fluorescence appeared not only as multiple punctae but also in a single, large focus. SMAP2 fluorescence was absent in elongated spermatids and sperm. Thus SMAP2 expression was stage dependent. Immunofluorescence localization of SMAP2 is consistent with the detection by Northern blot (Figure 1C).

We previously reported that SMAP2 was distributed on early endosomes (as multiple punctae) and on the TGN (as a single large focus) in tissue culture cells (Natsume *et al.*, 2006; Funaki *et al.*, 2011). Therefore we examined whether SMAP2 is similarly localized in spermatogenesis. Double-labeling immunofluorescence was performed on pachytene spermatocytes and round spermatids (Figure 3B). In the single large focus of SMAP2 staining, fluorescence from SMAP2 overlapped with that from TGN38, syntaxin6, and clathrin. Pearson's r was significant ($r > 0.5$) for each combination. In tissue culture cells, clathrin is located on various organelles but is particularly concentrated on the TGN (Huang *et al.*, 2007; Burgess *et al.*, 2011); TGN38 and syntaxin6 are TGN markers (Humphrey *et al.*, 1993; Bock *et al.*, 1997; Roqueta-Rivera *et al.*, 2011). Therefore the single, large, focus-like structure seen in germ cells most likely represents the TGN, and SMAP2 appears to be densely localized there. By contrast, GM130 is a marker of the *cis*-Golgi (Nakamura *et al.*, 1995), and fluorescence from SMAP2 and GM130 did not colocalize ($r < 0.5$). Furthermore, GM130 was located relatively far from the nucleus, whereas SMAP2 was relatively nearer to the nucleus, and this relative localization of SMAP2/TGN and GM130/*cis*-Golgi is in good accord with the known spatial orientation of the Golgi apparatus during spermiogenesis. Namely, rotation of the Golgi relocates the *cis*-Golgi and TGN so that they are oriented toward the cell surface and nucleus, respectively (Hermo *et al.*, 1980).

Aberrant acrosome formation in *SMAP2*-targeted spermiogenesis

We examined the relationship between SMAP2 residing on the TGN and acrosome formation. Acrosome formation occurs in the round and elongated spermatid stages and is divided into the following four phases: a Golgi phase, a cap phase, an acrosome phase, and a maturation phase (Figure 4A). Each phase is characterized by distinct staining patterns of the acrosomal component sp56 (Kim *et al.*, 2001). SMAP2 fluorescence at the TGN was detected in the Golgi and cap phases, and sp56 fluorescence was detected near the nucleus, whereas SMAP2 fluorescence was relatively distant from the nucleus. SMAP2 and sp56 fluorescence did not overlap. This relative localization is consistent with the known spatial orientation of the TGN and the acrosome. SMAP2 fluorescence was not detected in the acrosome and maturation phases. Therefore TGN-associated SMAP2 was detected in the early phases of acrosome formation when acrosomal components are synthesized. The disappearance of SMAP2 probably reflects the shedding of the TGN and other organelles during spermiogenesis (Susi *et al.*, 1971).

Many *SMAP2*(–/–) sperm exhibited globozoospermia, which is closely associated with aberrant acrosome formation (Holstein *et al.*, 1973; Ito *et al.*, 2004; Lin *et al.*, 2007; Roqueta-Rivera *et al.*, 2011). Therefore we examined acrosome formation during *SMAP2*(–/–) spermiogenesis using sp56 as a marker (Figure 4B). Various morphological abnormalities were evident in round and elongated spermatids. In Figure 4B, I, sp56 was not concentrated or fused into one focus but was distributed as multiple discrete spots along the nucleus; sp56 did not form a distinct cap over the nucleus and appeared to consist of a thick aggregate of multiple punctae (Figure 4B, II). The acrosome did not form the typical crescent but was irregular in shape (Figure 4B, III) and often remained separated into discrete foci (Figure 4B, IV). Therefore the *SMAP2* deficiency clearly perturbs acrosome formation. At the light microscopic level, the major perturbation appears to be abnormal fusion of the vesicles carrying the acrosomal components.

To correlate the abnormalities in the acrosome to the phases of acrosome formation, we frozen sectioned testis tissues and stained them with peanut agglutinin (PNA), a lectin that reacts with polysaccharides in the acrosome. Supplemental Figure S2A shows the Golgi

SMAP2 genotype	Number of mice examined	Number of sperm in epididymis ($\times 10^7$)	Number of sperm examined per mouse	Hook-shaped head (%)	Cylindrical or round head (%)
(–/–)	7	3.27 ± 0.68	57	21 ± 16	79 ± 16
(+/–)	4	3.27 ± 0.57	60	94 ± 6.8	6 ± 6.8
p	–	–	–	1E-05	1E-05

TABLE 2: Number of sperm and their morphology.

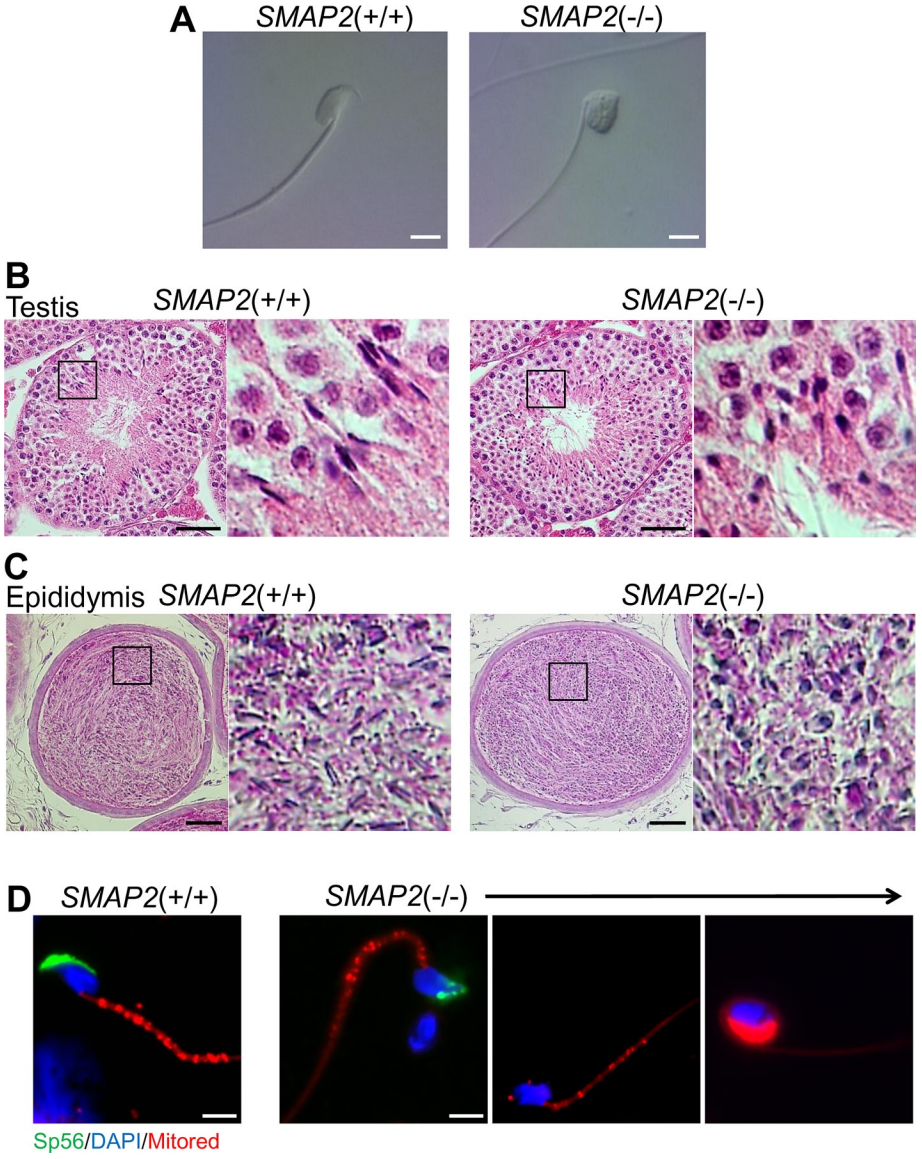

FIGURE 2: Morphology of sperm and spermatids in the epididymis and testis. (A) Sperm were collected from the epididymis of *SMAP2*(+/+) and (–/–) mice and observed using DIC microscopy. (B, C) Testis and epididymis specimens from *SMAP2*(+/+) and (–/–) mice were sectioned, stained with hematoxylin–eosin, and viewed using a light microscope. (D) Sperm from *SMAP2*(+/+) and (–/–) mice were stained with anti-sp56, DAPI, and MitoRed. Bars, 5 μm (A, D), 50 μm (B, C).

through the maturation phase in *SMAP2*(+/+) and (–/–) seminiferous tubules, and confirms the aberrant acrosome formation in *SMAP2*(–/–) cells. Periodic acid-Schiff stain (PAS) staining also revealed the presence of normal-shaped acrosomes in the elongated spermatids from the wild-type but not *SMAP2*(–/–) seminiferous tubules (Supplemental Figure S2B).

Formation of proacrosomal vesicles from the TGN is disrupted in *SMAP2*-targeted spermiogenesis

Acrosome formation is initiated by the budding of proacrosomal vesicles from the TGN. To examine possible abnormalities in this step, we processed testes sections for analysis by transmission electron microscopy (TEM; Figure 5A). In the Golgi phase of acrosome formation, wild-type spermatids (Figure 5A, I) possess an umbrella-shaped TGN, and multiple proacrosomal vesicles of uniform size are present between the TGN and nuclear membrane. By contrast, in *SMAP2*-targeted spermatids (Figure 5A, II), proacrosomal vesicles were present but were not uniform in size and appeared to be larger than those in wild-type cells. In other *SMAP2*-targeted spermatids (Figure 5A, III), the lamellar structure of the TGN formed loose whorls. These observations suggest that there are abnormalities in the budding of vesicles from the TGN in *SMAP2*-targeted cells.

To evaluate the foregoing observations more quantitatively, we measured the diameter of proacrosomal vesicles on the TEM sections. Approximately 20 vesicles per cell and a total of 15 cells were measured for each genotype. Figure 5B (also see Supplemental Figure S3) shows the range of proacrosomal vesicle sizes and confirms that the *SMAP2*-targeted cells tended to produce larger-diameter vesicles than do wild-type cells. Therefore abnormal acrosome formation in *SMAP2*-targeted cells appears to involve budding of proacrosomal vesicles from the TGN.

Formation of the acrosome from proacrosomal vesicles is disrupted in *SMAP2*-targeted spermiogenesis

The later phases of acrosome formation were examined by TEM (Figure 6). In the cap phase in wild-type cells (Figure 6, I), proacrosomal vesicles that had budded from the TGN fused with each other and formed a large acrosome (Ac) located at the acroplaxome (Apx), a unique substructure composed of keratin and actin that serves as a site for anchoring the acrosome to the nuclear membrane (Kierszenbaum *et al.*, 2003). By contrast, in a cap-phase *SMAP2*-targeted cell (Figure 6, II), acrosomes of intermediate size were formed but never fused to form one large acrosome and remained as multiple pseudoacrosomes (indicated by the arrows). These pseudoacrosomes attached to multiple sites on the nuclear envelope. In another *SMAP2*-targeted cell (Figure 6, III), one acrosome appeared to be formed but was greatly enlarged in size (the TGN was also disorganized and partly distended; arrows). These observations indicate that acrosome formation from proacrosomal vesicles in *SMAP2*-deficient cells is disrupted, even though the acroplaxome structures are well organized on the nuclear lamina. Therefore it is unlikely that a defect in the acroplaxome caused the aberrant acrosome formation.

Secondary abnormalities in spermiogenesis in *SMAP2*-deficient cells

In the acrosome phase in wild-type cells (Figure 6, IV), the acrosome was detected as a long and continuous layer along the nuclear membrane. In the enlargement of marginal rings (arrowhead), ectoplasmic specializations (two white arrows) derived from Sertoli cells cover the surface of the acrosome. A manchette structure is also

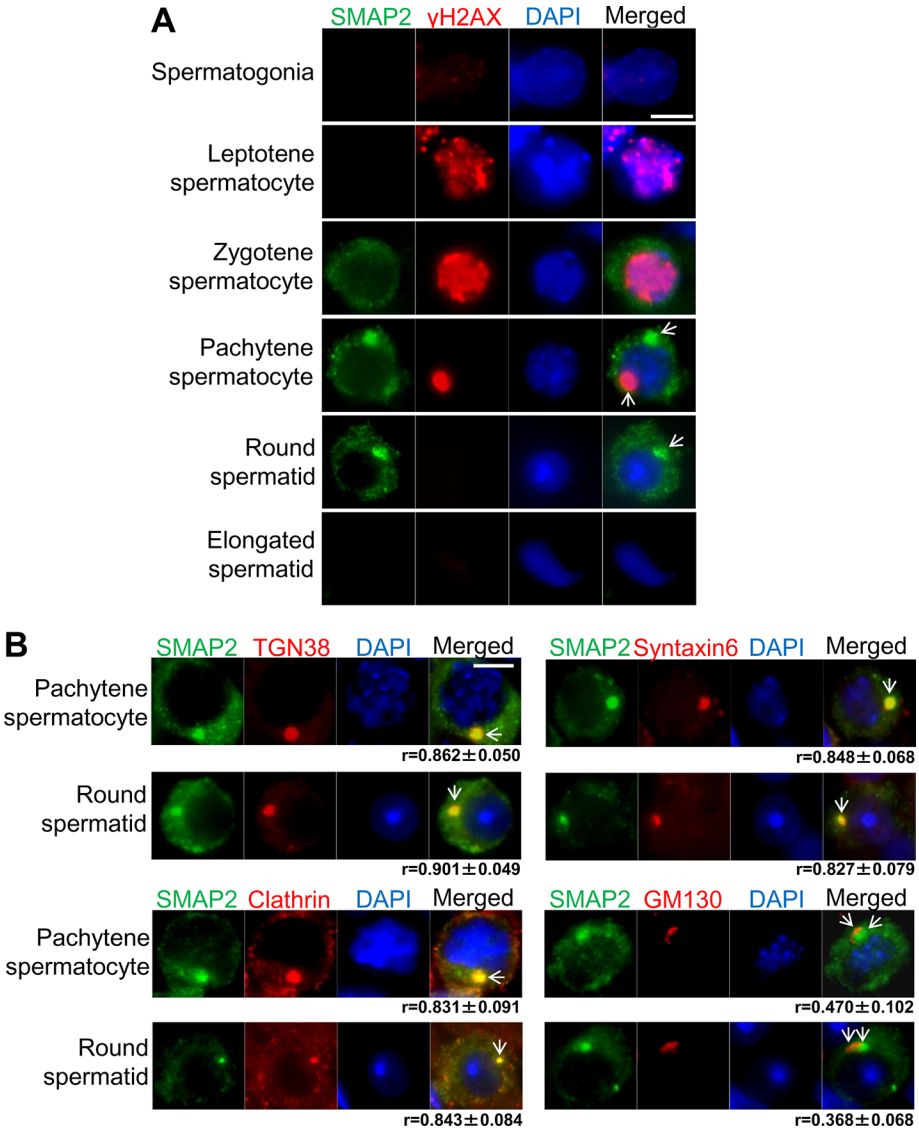

FIGURE 3: Expression and subcellular location of SMAP2 during spermatogenesis as detected by immunofluorescence staining. Single-cell suspensions were prepared from seminiferous tubules of wild-type testes, centrifuged onto glass slides, and fixed. (A) The cells were stained with anti-SMAP2, anti-γH2AX, and DAPI. Based on the staining pattern of the nuclear γH2AX and DAPI, differentiation stages were assigned as indicated. (B) The cells were stained as indicated. Pachytene spermatocytes and round spermatids are shown. Clathrin is the vesicle marker, TGN38 and syntaxin6 are TGN markers, and GM130 is a *cis*-Golgi marker. Bar, 5 μm. Values of *r* (average ±SD) represent the Pearson's coefficients quantifying the degree of colocalization between SMAP2 and the various marker proteins. For $r > 0.5$, colocalization is significant.

observed (asterisk). In a *SMAP2*(–/–) cell (Figure 6, V), however, the ectoplasmic specializations were interrupted (arrow), and the acrosome appeared swollen near the marginal ring (arrowhead). In another *SMAP2*(–/–) cell (Figure 6, VI), a space between the acrosome and nucleus appeared to be filled with a Sertoli cell protrusion (Sc; arrow).

Finally, in the maturation phase in wild-type cells (Figure 6, VII), the ectoplasmic specialization (two white arrows) and the manchette (asterisk) were observed, but in a *SMAP2*(–/–) cell (Figure 6, VIII), the nucleus appeared fragmented, the acrosome was dispersed (arrows), and the manchette was located ectopically (asterisk). An invagination of the manchette into the nucleus was observed in another *SMAP2*(–/–) cell (Figure 6, IX). Finally, in *SMAP2*(–/–) sperm from the epididymis, the shedding of cytoplasmic content appeared to be incomplete, since many mitochondria were detected near the nucleus (Figure 6, XI). These alterations in the acrosome and maturation phases in *SMAP2*-deficient sperm may be secondary events that result from the defects in proacrosomal vesicle budding and acrosome formation.

Molecules involved in the formation of proacrosomal vesicles

The proacrosomal vesicles budding from the TGN in *SMAP2*(–/–) spermatids had larger diameters than those in the wild-type cells (Figure 5). CALM is a protein that affects the size of clathrin-coated vesicles, since vesicles become enlarged in cells lacking *CALM/AP180* (Zhang *et al.*, 1998; Nonet *et al.*, 1999; Meyerholz *et al.*, 2005). In addition, we previously reported a physical association between SMAP2 and CALM (Natsume *et al.*, 2006). Therefore, to explore a possible link between SMAP2 and the vesicle size, we performed double immunofluorescence of SMAP2 and CALM using a germ cell suspension (Figure 7A). In wild-type spermatocytes and round spermatids, SMAP2 was concentrated at the TGN, as described earlier, whereas CALM fluorescence was detected diffusely in the cytoplasm but also colocalized with SMAP2. In the *SMAP2*(–/–) cells, CALM was no longer localized to the TGN (the overall amount of CALM was not affected by SMAP2 deficiency; data not shown). When the wild-type and *SMAP2*(–/–) germ cells were mixed at a 1:1 ratio, CALM was colocalized with SMAP2 at the TGN in the wild-type cells but homogenously distributed in the *SMAP2*(–/–) cells. Thus mobilization of CALM to the TGN appears to be dependent on SMAP2.

We also used coimmunoprecipitation to confirm a physical association between SMAP2 and CALM (Figure 7B). Lysates were prepared from wild-type testes and immunoprecipitated with an anti-CALM antibody. Immunoblotting of the precipitate with an anti-SMAP2 antibody revealed the presence of SMAP2, indicating an association between CALM and SMAP2.

An important implication of the observations of acrosome formation (Figure 6) is that some process in the fusion of proacrosomal vesicles was impaired in the *SMAP2*(–/–) cells. Syntaxin2 is a component of the soluble *N*-ethylmaleimide–sensitive factor attachment protein receptor (SNARE) complex, which serves as the fusion machinery for proacrosomal vesicles (Rizo and Sudhof, 2002; Roqueta-Rivera *et al.*, 2011). In Figure 7C, cells were double stained for syntaxin2 and sp56. In wild-type spermatocytes, syntaxin2 was concentrated at foci in the cytoplasm. In round spermatids, syntaxin2 was detected adjacent to the sp56 fluorescence. In contrast, in the *SMAP2*(–/–) cells, although syntaxin2 was concentrated at foci during the spermatocyte stage, during the round spermatid stage

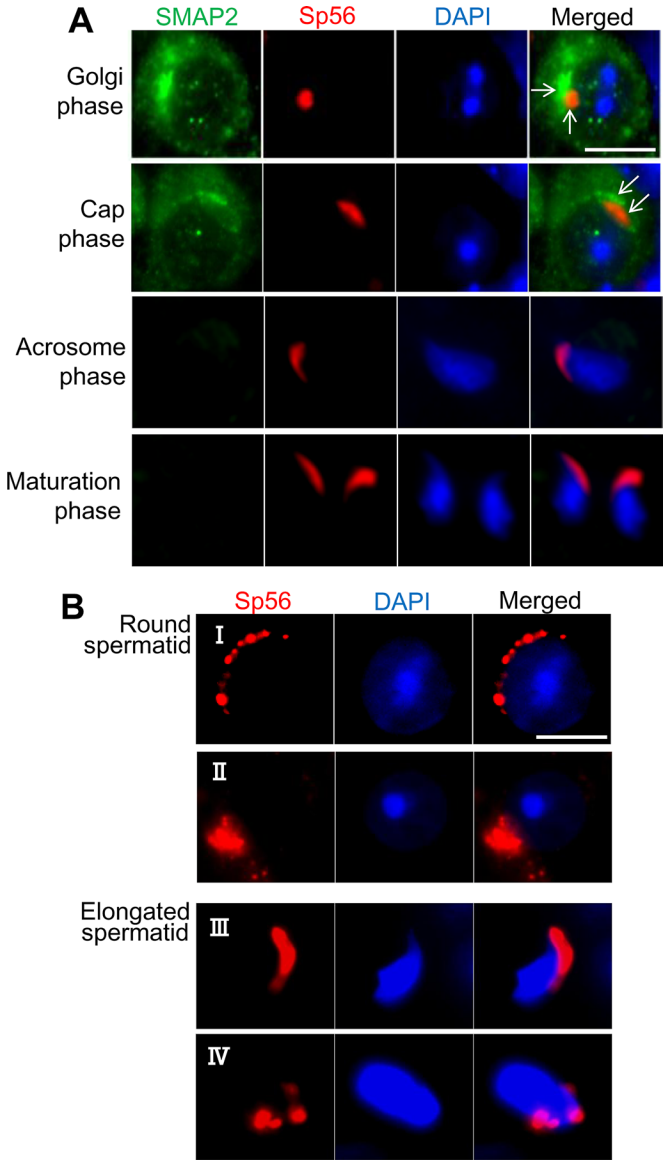

FIGURE 4: Acrosome formation and SMAP2. (A) Germ cells were prepared from wild-type testes as in Figure 3 and processed for immunofluorescence staining as indicated. Each row represents a stage of acrosome formation (Golgi, cap, acrosome, and maturation phases). The marker for the acrosomal components is sp56. (B) Germ cells were prepared from *SMAP2*(–/–) testes and processed for sp56 staining. See the text for details of observed abnormalities. Bars, 5 μm.

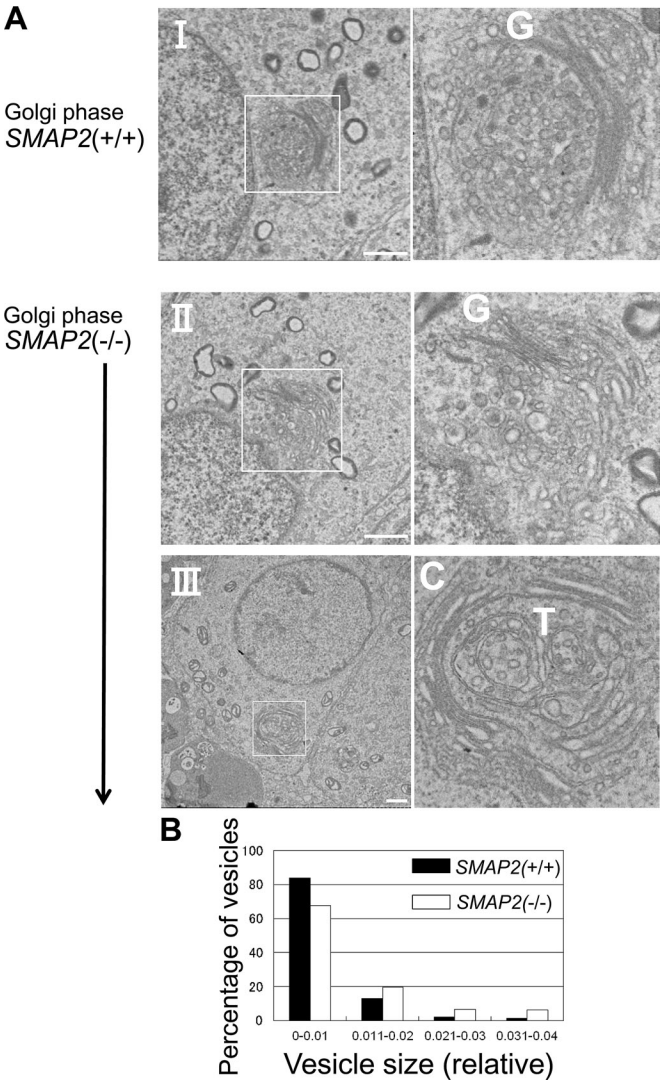

FIGURE 5: Electron microscopic observations of proacrosomal vesicle formation at the Golgi phase. (A) Germ cells from *SMAP2*(+/+) and (–/–) mice were processed for electron microscopic observations. C, *cis*-Golgi network; G, Golgi apparatus; T, *trans*-Golgi network. Bars, 1 μm. (B) Size distribution of proacrosomal vesicles observed in *SMAP2*(+/+) (closed bars) and (–/–) (open bars) germ cells at the Golgi phase. Using the images shown in A, we measured diameters for each proacrosomal vesicle. The areas of the vesicles were calculated using image-processing software and divided by the square of the magnification. The diameters are presented in relative units. Vesicle sizes are binned as indicated. See Supplemental Figure S3 for the detailed size distribution of vesicles.

syntaxin2 was irregularly distributed in the cytoplasm and had no discernible correlation with sp56 fluorescence. This result suggests that the SNARE complex may not be properly engaged in the fusion events in *SMAP2*-deficient germ cells. Syntaxin2 was not detected in CALM immunoprecipitates of wild-type cells (Figure 7B).

Finally, the relative orientation of syntaxin2 to TGN38 was examined by double labeling (Figure 7D). In wild-type spermatocytes, focal fluorescence of syntaxin2 partly overlapped with that of TGN38. In wild-type round spermatids, syntaxin2 localization was distinct from TGN38. Of note, syntaxin2 was located closer to the nucleus, whereas TGN38 was detected further from the nucleus. The observations are consistent with the scenario that syntaxin2 originates from the TGN and then moves to the site of proacrosomal vesicle fusion. Such features were never observed in *SMAP2*(–/–) spermatids.

DISCUSSION

In this study we showed that *SMAP2*-deficient male mice are infertile. Sperm in the testes and epididymides in these mice exhibit morphological abnormalities indicative of globozoospermia, a phenotype seen also in infertile men. Formation of the acrosome is disrupted in *SMAP2*-deficient sperm, and several reports suggested that defects in acrosome formation cause globozoospermia (Holstein *et al.*, 1973; Ito *et al.*, 2004; Lin *et al.*, 2007; Roqueta-Rivera *et al.*, 2011). Therefore the globozoospermia seen in the *SMAP2* deficiency is likely due to defects in acrosome formation.

During spermiogenesis, a large number of proacrosomal vesicles bud from the TGN, fuse with each other, anchor to the nuclear

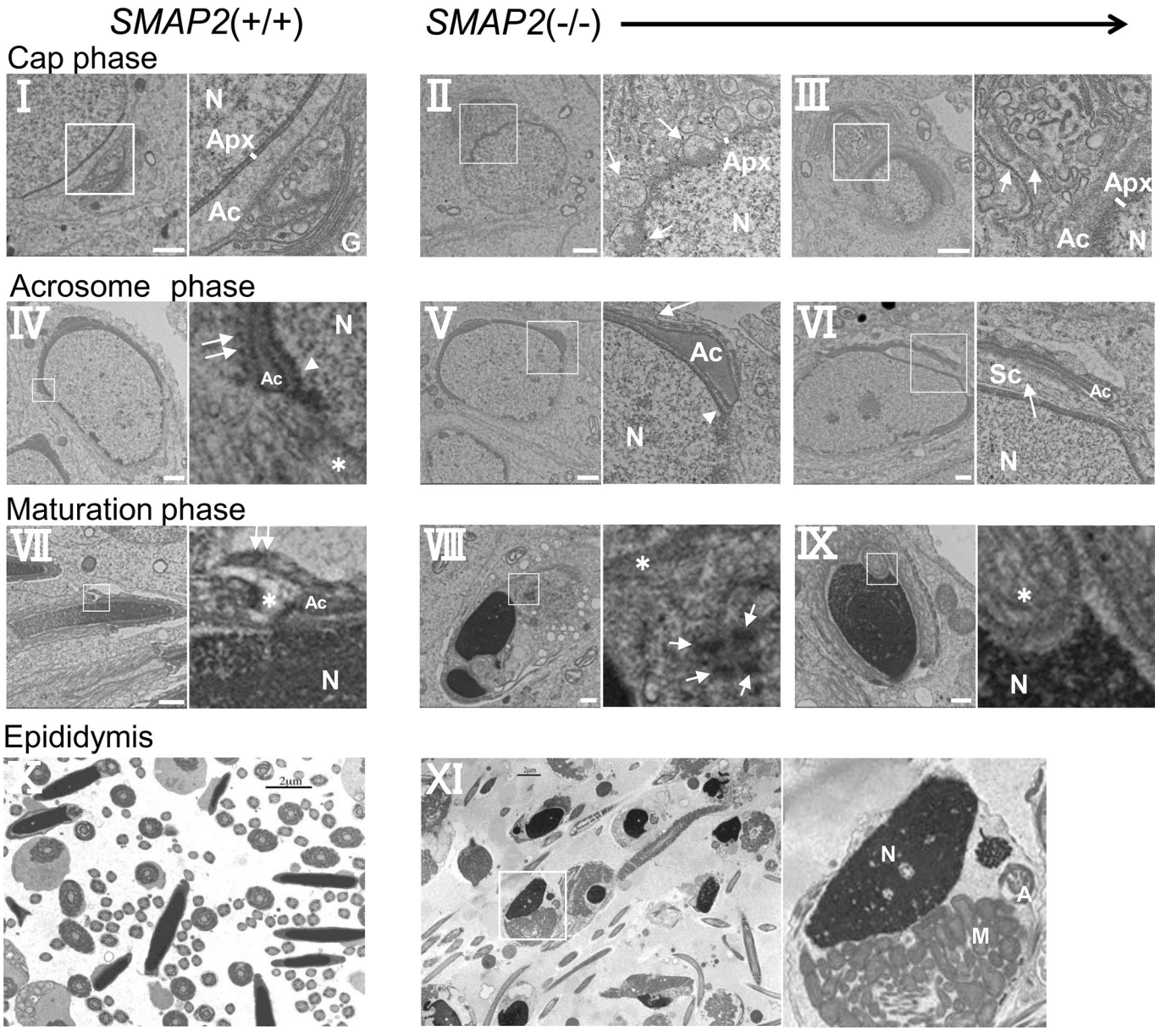

FIGURE 6: Electron microscopic observations of acrosome formation and subsequent events in wild-type and *SMAP2*-targeted germ cells. Cells at the cap, acrosome, and maturation phases of acrosome formation are shown. Sections of epididymides are also shown. See the text for the description of structural abnormalities. A, axoneme; Ac, acrosome; Apx, acroplaxome; G, Golgi apparatus; M, mitochondria; N, nucleus; Sc, Sertoli cell. Arrowheads in IV and V are marginal rings. Asterisks in IV and VII–IX are manchettes. Double white arrows in IV and VII are ectoplasmic specializations derived from Sertoli cells. White arrows indicate pseudoacrosomes (II), a disorganized TGN structure (III), interrupted ectoplasmic specializations (V), invagination of a Sertoli cell into the germ cell (VI), and fragmented acrosomes (VIII). Bars, 1 μm (I–IX), 2 μm (X, XI).

membrane, and eventually form a large organelle known as the acrosome (Abou-Haila and Tulsiani, 2000; Moreno and Alvarado, 2006). We reported previously that SMAP2 is located on the TGN and functions in vesicle transport from the TGN in tissue culture cells such as HeLa and Cos7 cells (Funaki *et al*., 2011). These results suggested that SMAP2 might be directly involved in the budding of proacrosomal vesicles from the TGN in spermatogenesis. This hypothesis is supported by the following observations. 1) SMAP2 protein is detected in wild-type germ cells and in the pachytene spermatocyte to the round spermatid stages. Acrosomal proteins are actively synthesized at the pachytene stage (Anakwe and Gerton, 1990), and enormous amounts of proacrosomal vesicles are supplied from the TGN until the round spermatid stage. Thus the observed pattern of SMAP2 expression coincides with the period of acrosome formation. 2) In wild-type spermatogenic cells, SMAP2 is located exclusively on the TGN. 3) In *SMAP2*-deficient germ cells, the TGN tend to lose structural integrity, appearing as loose whorls, and the diameters of proacrosomal vesicles become significantly larger than in wild-type cells.

The primary alteration in spermiogenesis in *SMAP2*-deficient mice was the enlargement of the proacrosomal vesicles, suggesting that this change may ultimately cause the globozoospermic morphology. In other words, SMAP2 may function to standardize

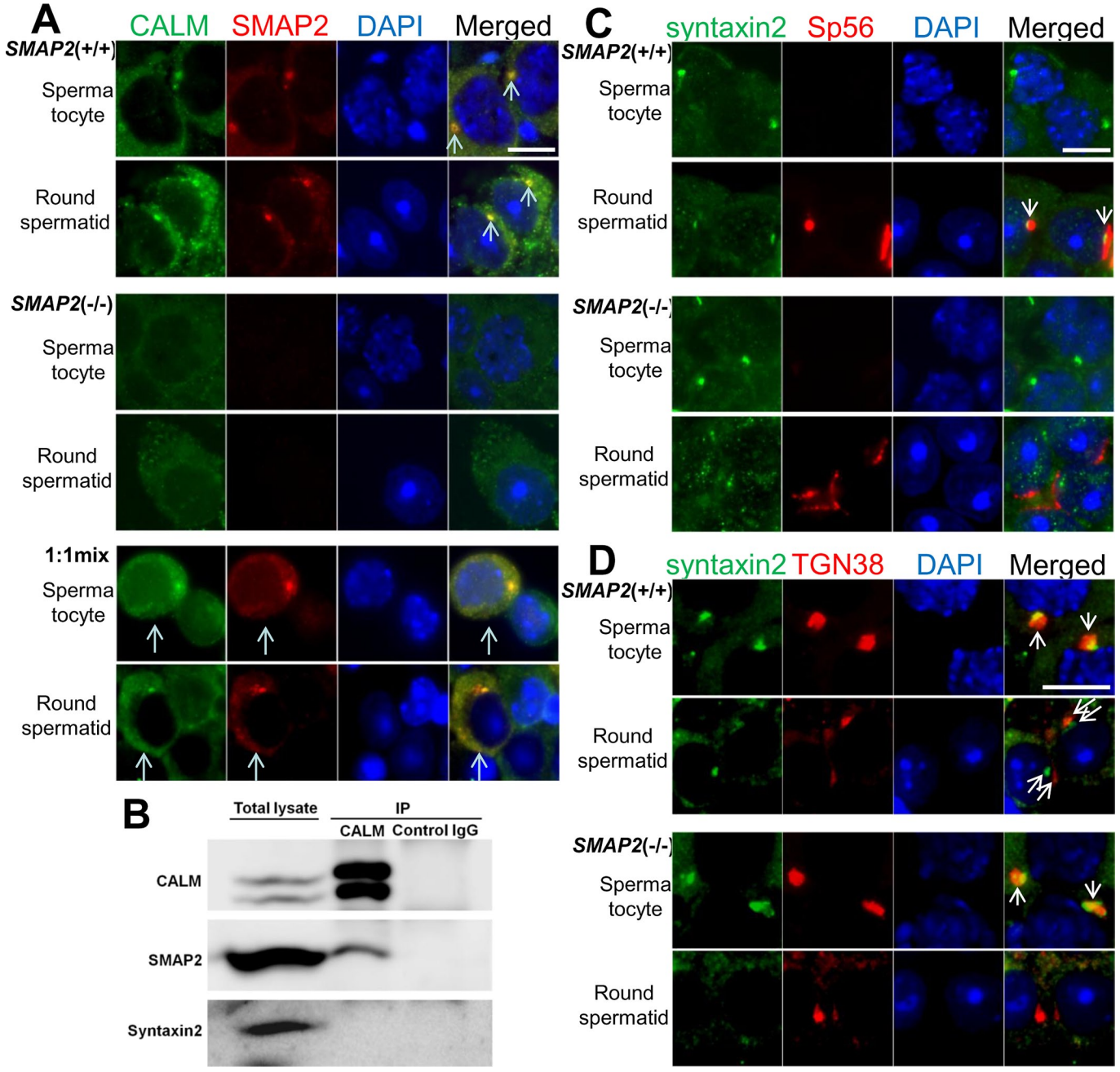

FIGURE 7: Subcellular localization of CALM and syntaxin2 as revealed by immunofluorescence staining. (A, C, D) *SMAP2*(+/+) and (–/–) germ cells were prepared as in Figure 3 and stained with anti-SMAP2, anti-CALM, anti-syntaxin2, anti-sp56, anti-TGN38, and DAPI, as indicated. The 1:1 mix is a mixed sample of *SMAP2*(+/+) and (–/–) cells. Pachytene spermatocytes and round spermatids are shown. Bar, 5 µm. (B) Immunoprecipitation of CALM. Lysates prepared from wild-type testes were immunoprecipitated with an anti-CALM antibody, and the precipitates were blotted with anti-CALM, anti-SMAP2, or anti-syntaxin2, as indicated.

the size of TGN-derived vesicles. Thus a principal issue is how SMAP2 might function to regulate vesicle size during vesicle formation. CALM and its homologue, AP180, control the size of clathrin-coated vesicles. When *CALM/AP180* is abolished, vesicles become enlarged (Zhang *et al.*, 1998; Nonet *et al.*, 1999; Meyerholz *et al.*, 2005), similar to the effects of *SMAP2* deficiency. We reported previously that SMAP2 binds to CALM directly (Natsume *et al.*, 2006). One possible scenario for *SMAP2* deficiency is that CALM is not recruited to the site of vesicle formation, thus causing the vesicle size to be unregulated. Consistent with this hypothesis, CALM is detected at the TGN in wild-type but not in *SMAP2*(–/–) cells.

In addition to the morphological abnormalities, *SMAP2*(–/–) proacrosomal vesicles may have other functional defects. Vesicle-associated membrane proteins (VAMPs) are components of the SNARE complex, and CALM can function to recruit some VAMPs to clathrin-coated vesicles through physical association with the VAMPs (Harel *et al.*, 2008; Koo *et al.*, 2011; Miller *et al.*, 2011). Therefore recruitment of SNARE complex components may be defective in *SMAP2*-deficient proacrosomal vesicles, since CALM was not

concentrated at the TGN. Although the association of CALM and syntaxin2 was not detected in lysates of wild-type cells, we did observe a rather irregular localization of syntaxin2 in *SMAP2*(–/–) cells. Such alterations in the composition of proacrosomal vesicles might be related to the apparent defect in fusion of proacrosomal vesicles into an acrosomal structure that resulted in the generation of nonfused, segmented acrosomes. The present study therefore suggests a scenario in which the budding and fusion of proacrosomal vesicles are linked by the recruitment of specific proteins to the vesicles.

Malformation of the acrosome causes secondary effects on the manchette (Kierszenbaum *et al.*, 2004; Pierre *et al.*, 2012). In particular, the manchette cannot be localized to the perinuclear ring; thus the manchette–acrosome connection becomes disorganized, and spermatid–Sertoli cell adhesion is perturbed (Kierszenbaum *et al.*, 2007). In *SMAP2*-deficient spermatids, the manchette was sometimes mislocalized, and the ectoplasmic specializations from the Sertoli cells were not formed properly, or the anchoring of the acrosome to the nucleus appeared weak, thus allowing invagination of the Sertoli cells into the spermatid. Thus, in *SMAP2*-deficient spermatogenesis, both primary defects in proacrosomal vesicle formation and secondary defects in manchette attachment likely contribute to the abnormal globozoospermic morphology (Kierszenbaum and Tres, 2004; Kierszenbaum *et al.*, 2011; Fujihara *et al.*, 2012).

Endocytosis of cell membrane proteins also contributes to the formation of the acrosome (Moreno and Alvarado, 2006; Berruti *et al.*, 2010; Rainey *et al.*, 2010; Paiardi *et al.*, 2011). Our previous study using cell lines showed that SMAP2 is located on early endosomes (Natsume *et al.*, 2006). Therefore we cannot exclude the possibility that some defects in retrograde traffic from early endosomes to the TGN might also be involved in the genesis of the globozospermia seen in *SMAP2*(–/–) mice.

There are several mouse models reported to exhibit abnormalities in proacrosomal vesicle formation from the TGN. In gene-targeted mice with knockouts of HIV-Rev-binding protein (*Hrb*), Golgi-associated PDZ and coiled-coil motif-containing protein (*GOPC*), Hook homologue 1 (*Hook1*), or protein interacting with C kinase 1 (*Pick1*), acrosome formation is defective. All of these molecules are involved in the transport of proacrosomal vesicles from the TGN (Kang-Decker *et al.*, 2001; Yao *et al.*, 2002; Moreno *et al.*, 2006; Xiao *et al.*, 2009; Kierszenbaum *et al.*, 2011). Among these knockouts, Hrb belongs to an Arf GAP family, as does SMAP2. *Hrb*-deficient male mice exhibit globozoospermia, but the details of the phenotype appear distinct from *SMAP2*-deficient spermatogenesis. In *Hrb*-deficient mice, the number of mature sperm is extremely low, some sperm possess multiple nuclei due to a defect in meiosis, and other sperm possess multiple flagella due to an increased number of centrioles (Juneja and van Deursen, 2005). These features were not observed in *SMAP2*-deficient spermiogenesis. Furthermore, Hrb plays a role distinct from SMAP2, in that the Hrb protein is located on the cytoplasmic side of the proacrosomal vesicles and functions in their fusion. Thus, although both SMAP2 and Hrb are Arf GAPs and their deficiencies cause globozoospermia, the two proteins appear to exert nonoverlapping, unique functions during spermatogenesis.

MATERIALS AND METHODS

Generation of *SMAP2*-targeted mice

A lambda phage clone encompassing exon 1 of *SMAP2*, which contains the methionine start codon, was isolated from a 129/SvJ genomic library (Stratagene, Santa Clara, CA). A targeting vector was constructed in which a fragment containing the *LacZ* and *PGK-neo*^{R} sequences was inserted into the *Kpn*I site of exon 1, and a *diphtheria toxin-A*–encoding fragment was ligated at the 5′ end. The vector was linearized by *Not*I digestion and electroporated into E14 ES cells. Of 610 G418-resistant clones, five were judged to have undergone proper homologous recombination based on PCR and Southern blot analysis of genomic DNA. Procedures for PCR and Southern blotting were as previously described (Wong *et al.*, 2010). Cells with a normal karyotype were selected using a Colcemid treatment method. Three ES cell clones were injected into blastocysts, and the chimeric males that were produced were mated with C57BL/6J female mice. Finally, two lines of *SMAP2*(+/–) founder mice were established that possessed the *SMAP2*-targeted allele in the germline. PCR primers used for genotyping were as follows. To detect the wild-type allele, the forward and reverse primers were 5′-CACTCGGGGTCAAGTGTGCG-3′ and 5′-CCAGAACCCCCTCCCCACTC-3′, respectively. To detect the targeted allele, the forward and reverse primers were 5′-CGCCTTCTATCGCCTTCTTGACG-3′ and 5′-CTTTCCGCCTCAGAAGCCATAGAG-3′, respectively.

In vitro fertilization and intracytoplasmic sperm injection

For in vitro fertilization, mature oocytes were collected from oviducts of B6D2F1 female mice that had been superovulated by the injection of 5 IU each of equine and human chorionic gonadotrophin. Sperm were collected from the epididymides of *SMAP2*(+/–) or (–/–) male mice. In each experiment, oocytes from two females were incubated with sperm from one male at a concentration of 200 sperm/μl. Fertilization was confirmed by development to the two-cell stage by 24 h after insemination.

For intracytoplasmic sperm injection, germ cells were collected from seminiferous tubules of *SMAP2*(+/–) or (–/–) testes. Elongated spermatids that were at differentiation steps 9–11 were picked up and injected into oocytes using a piezo-driven micromanipulator (PrimeTech, Tsuchiura, Japan). Oocytes that survived injection were cultured in a potassium simplex optimized medium, and those that developed to the two-cell stage were transplanted into oviducts of pseudopregnant ICR female mice. The offspring were counted at full term, namely, on day 19.5, by caesarian section or after natural delivery.

Transplantation of spermatogonial stem cells

Four-week-old WBB6F1-W/W^v mice that were devoid of spermatogenic cells were purchased from Japan SLC (Hamamatsu, Japan) and used as recipient animals. Spermatogonial stem cells were prepared from *SMAP2*(–/–) testes by a two-step enzymatic digestion technique as described previously (Ogawa *et al.*, 1997). A volume of 10 μl of spermatogenic cells, (2–3) × 10^7 cells/ml, was introduced into the seminiferous tubules of the WBB6F1-W/W^v mouse testis. As a control experiment, spermatogonial stem cells of *SMAP2*(+/+) mice were transplanted into *SMAP2*(–/–) mice. For recipient preparation, busulfan (44 mg/kg body weight) was injected intraperitoneally into 3-wk-old *SMAP2*(–/–) male mice. After 6 wk, the busulfan-treated testes were devoid of endogenous spermatogenesis. Spermatogonial stem cells were prepared from the testes of pCXN-EGFP transgenic, *SMAP2*(+/+) male mice (Okabe *et al.*, 1997) and introduced into the seminiferous tubules of the busulfan-treated *SMAP2*(–/–) mice.

At 3 mo posttransplantation, mice were killed and testes were removed. The seminiferous tubules were dissected out of the testes, and sperm released from the tubules was observed with an Olympus BX50 microscope (Olympus, Tokyo, Japan) using DIC optics. The tubules were transferred into a fixative containing 2.5% (wt/vol) glutaraldehyde in 0.1 M phosphate buffer, pH 7.4, and processed for microscopic observation.

Histology and immunofluorescence detection

Testes were fixed in Bouin's solution, embedded in paraffin, and sectioned. Deparaffinized sections were stained with hematoxylin and eosin, toluidine blue, or PAS, according to standard procedures. Some testes were fixed in 4% (wt/vol) paraformaldehyde in phosphate-buffered saline (PBS), immersed in 20% (wt/vol) sucrose in PBS, frozen in an optimal cutting temperature compound, cryostat sectioned, and processed for immunofluorescence. For some samples, germ cells were liberated as single-cell suspensions from testes or epididymides, centrifuged onto slide glasses, fixed, and processed for immunofluorescence. The following antibodies were used: anti-SMAP2 (Sigma-Aldrich, St. Louis, MO), anti-γH2AX (Trevigen, Gaithersburg, MD), anti-TGN38 (AbD Serotec, Raleigh, NC), anti–clathrin heavy chain (Affinity BioReagents, Golden, CO), anti-syntaxin6 (BD Transduction Labs, Lexington, KY), anti-GM130 (BD Transduction Labs), anti-sp56 (QED Bioscience, San Diego, CA), anti-syntaxin2 (Abcam, Cambridge, MA), anti-CALM (Santa Cruz Biotechnology, Santa Cruz, CA), and appropriate fluorophore-conjugated secondary antibodies. Rhodamine-conjugated PNA and MitoRed were obtained from Vector Laboratories (Burlingame, CA) and Dojindo (Rockville, MD), respectively. Fluorescence was observed using a BZ9000 fluorescence microscope (Keyence, Osaka, Japan). The Pearson's *r* quantifying the colocalization between images was calculated using the JACoP plug-in in ImageJ (National Institutes of Health, Bethesda, MD).

Electron microscopic observations

Mice were killed and perfused with a fixative containing 2.5% (wt/vol) glutaraldehyde in 0.1 M phosphate buffer, pH 7.4. Testes and epididymides were removed and treated with the same fixative at 4°C overnight. Tissues were cut into small pieces, rinsed, and postfixed in 1% (wt/vol) OsO_4 in distilled water for 1 h. The samples were dehydrated using increasing concentrations of ethanol and embedded in Epon 812. The plastic-embedded tissues were sectioned using an ultramicrotome (model Ultracut E; Reihert-Jung, Vienna, Austria) and stained with uranyl acetate and lead citrate. The samples were observed using a JEOL 1200 EX transmission electron microscope (JEOL, Tokyo, Japan).

Northern blot, immunoblot, and immunoprecipitation analyses

RNA was isolated from cells/tissues of C57BL/6J mice using TRIzol (Life Technologies, Carlsbad, CA). When necessary, germ cells from testes were fractionated into various differentiation stages by centrifugal elutriation (Barchi *et al.*, 2009). For Northern blots, 10 µg of total RNA was separated in a 1% (wt/vol) formaldehyde/agarose gel and transferred to a Hybond membrane (Amersham, Piscataway, NJ), according to the manufacturer's instructions. The filter was hybridized with a radiolabeled *Sph*I fragment of *SMAP2* cDNA.

Protein lysates of cells/tissues were prepared with a Polytron homogenizer using a buffer containing 9 M urea, 2% (vol/vol) Triton X-100, and 1% (wt/vol) dithiothreitol. The lysates were centrifuged at 13,000 rpm for 15 min, and the supernatant was collected. Lithium dodecyl sulfate was added to a final concentration of 2% (wt/vol), and the solution was sonicated. The protein concentration was determined using a Bio-Rad (Hercules, CA) protein assay kit. Protein samples (20 µg) were separated on an 8% SDS–PAGE gel and electrotransferred to a polyvinylidene fluoride membrane (Millipore, Billerica, MA). Immunoblotting was performed using anti–β actin (Sigma-Aldrich), anti-SMAP2, anti-CALM, or anti-syntaxin2 antibodies and an ECL reagent (Amersham). Some lysates were first immunoprecipitated, as described previously (Natsume *et al.*, 2006), and the precipitates were then blotted using one of the antibodies described.

Statistical analyses

Statistical significance was evaluated using a two-tailed Student's *t* test, and differences of $p < 0.05$ were considered statistically significant.

ACKNOWLEDGMENTS

This work was supported by Grants-in-Aid from the Ministry of Education, Science, Sports, Culture and Technology, Japan. M.S. is a member of the Global COE "Network Medicine" at Tohoku University.

REFERENCES

Abou-Haila A, Tulsiani DR (2000). Mammalian sperm acrosome: formation, contents, and function. Arch Biochem Biophys 379, 173–182.

Anakwe OO, Gerton GL (1990). Acrosome biogenesis begins during meiosis: evidence from the synthesis and distribution of an acrosomal glycoprotein, acrogranin, during guinea pig spermatogenesis. Biol Reprod 42, 317–328.

Barchi M, Geremia R, Magliozzi R, Bianchi E (2009). Isolation and analyses of enriched populations of male mouse germ cells by sedimentation velocity: the centrifugal elutriation. Methods Mol Biol 558, 299–321.

Berruti G, Ripolone M, Ceriani M (2010). USP8, a regulator of endosomal sorting, is involved in mouse acrosome biogenesis through interaction with the spermatid ESCRT-0 complex and microtubules. Biol Reprod 82, 930–939.

Bock JB, Klumperman J, Davanger S, Scheller RH (1997). Syntaxin 6 functions in *trans*-Golgi network vesicle trafficking. Mol Biol Cell 8, 1261–1271.

Bonifacino JS, Rojas R (2006). Retrograde transport from endosomes to the *trans*-Golgi network. Nat Rev Mol Cell Biol 7, 568–579.

Burgess J *et al.* (2011). AP-1 and clathrin are essential for secretory granule biogenesis in *Drosophila*. Mol Biol Cell 22, 2094–2105.

Dam AH, Feenstra I, Westphal JR, Ramos L, van Golde RJ, Kremer JA (2007). Globozoospermia revisited. Hum Reprod Update 13, 63–75.

Donaldson JG, Jackson CL (2011). ARF family G proteins and their regulators: roles in membrane transport, development and disease. Nat Rev Mol Cell Biol 12, 362–375.

D'Souza-Schorey C, Chavrier P (2006). ARF proteins: roles in membrane traffic and beyond. Nat Rev Mol Cell Biol 7, 347–358.

Ford WC (2006). Glycolysis and sperm motility: does a spoonful of sugar help the flagellum go round? Hum Reprod Update 12, 269–274.

Fujihara Y, Satouh Y, Inoue N, Isotani A, Ikawa M, Okabe M (2012). SPACA1-deficient male mice are infertile with abnormally shaped sperm heads reminiscent of globozoospermia. Development 139, 3583–3589.

Funaki T, Kon S, Ronn RE, Henmi Y, Kobayashi Y, Watanabe T, Nakayama K, Tanabe K, Satake M (2011). Localization of SMAP2 to the TGN and its function in the regulation of TGN protein transport. Cell Struct Funct 36, 83–95.

Gillingham AK, Munro S (2007). The small G proteins of the Arf family and their regulators. Annu Rev Cell Dev Biol 23, 579–611.

Harel A, Wu F, Mattson MP, Morris CM, Yao PJ (2008). Evidence for CALM in directing VAMP2 trafficking. Traffic 9, 417–429.

Hermo L, Rambourg A, Clermont Y (1980). Three-dimensional architecture of the cortical region of the Golgi apparatus in rat spermatids. Am J Anat 157, 357–373.

Holstein AF, Schirren C, Schirren CG (1973). Human spermatids and spermatozoa lacking acrosomes. J Reprod Fertil 35, 489–491.

Huang C, Chang SC, Yu IC, Tsay YG, Chang MF (2007). Large hepatitis delta antigen is a novel clathrin adaptor-like protein. J Virol 81, 5985–5994.

Humphrey JS, Peters PJ, Yuan LC, Bonifacino JS (1993). Localization of TGN38 to the *trans*-Golgi network: involvement of a cytoplasmic tyrosine-containing sequence. J Cell Biol 120, 1123–1135.

Ito C, Suzuki-Toyota F, Maekawa M, Toyama Y, Yao R, Noda T, Toshimori K (2004). Failure to assemble the peri-nuclear structures in GOPC deficient spermatids as found in round-headed spermatozoa. Arch Histol Cytol 67, 349–360.

Juneja SC, van Deursen JM (2005). A mouse model of familial oligoasthenoteratozoospermia. Hum Reprod 20, 881–893.

Kahn RA (2009). Toward a model for Arf GTPases as regulators of traffic at the Golgi. FEBS Lett 583, 3872–3879.
Kahn RA (2011). GAPs: Terminator versus effector functions and the role(s) of ArfGAP1 in vesicle biogenesis. Cell Logist 1, 49–51.
Kang-Decker N, Mantchev GT, Juneja SC, McNiven MA, van Deursen JM (2001). Lack of acrosome formation in Hrb-deficient mice. Science 294, 1531–1533.
Kierszenbaum AL, Rivkin E, Tres LL (2003). Acroplaxome, an F-actin-keratin-containing plate, anchors the acrosome to the nucleus during shaping of the spermatid head. Mol Biol Cell 14, 4628–4640.
Kierszenbaum AL, Rivkin E, Tres LL (2007). Molecular biology of sperm head shaping. Soc Reprod Fertil Suppl 65, 33–43.
Kierszenbaum AL, Rivkin E, Tres LL (2011). Cytoskeletal track selection during cargo transport in spermatids is relevant to male fertility. Spermatogenesis 1, 221–230.
Kierszenbaum AL, Tres LL (2004). The acrosome-acroplaxome-manchette complex and the shaping of the spermatid head. Arch Histol Cytol 67, 271–284.
Kierszenbaum AL, Tres LL, Rivkin E, Kang-Decker N, van Deursen JM (2004). The acroplaxome is the docking site of Golgi derived myosin Va/Rab27a/b- containing proacrosomal vesicles in wild-type and Hrb mutant mouse spermatids. Biol Reprod 70, 1400–1410.
Kim KS, Cha MC, Gerton GL (2001). Mouse sperm protein sp56 is a component of the acrosomal matrix. Biol Reprod 64, 36–43.
Kon S, Funaki T, Satake M (2011). Putative terminator and/or effector functions of Arf GAPs in the trafficking of clathrin-coated vesicles. Cell Logist 1, 86–89.
Kon S *et al.* (2013). Smap1 deficiency perturbs receptor trafficking and predisposes mice to myelodysplasia. J Clin Invest 123, 1123–1137.
Kon S, Tanabe K, Watanabe T, Sabe H, Satake M (2008). Clathrin dependent endocytosis of E-cadherin is regulated by the Arf6GAP isoform SMAP1. Exp Cell Res 314, 1415–1428.
Koo SJ, Markovic S, Puchkov D, Mahrenholz CC, Beceren-Braun F, Maritzen T, Dernedde J, Volkmer R, Oschkinat H, Haucke V (2011). SNARE motif-mediated sorting of synaptobrevin by the endocytic adaptors clathrin assembly lymphoid myeloid leukemia (CALM) and AP180 at synapses. Proc Natl Acad Sci USA 108, 13540–13545.
Lin YN, Roy A, Yan W, Burns KH, Matzuk MM (2007). Loss of zona pellucida binding proteins in the acrosomal matrix disrupts acrosome biogenesis and sperm morphogenesis. Mol Cell Biol 27, 6794–6805.
McMahon HT, Boucrot E (2011). Molecular mechanism and physiological functions of clathrin-mediated endocytosis. Nat Rev Mol Cell Biol 12, 517–533.
Meyerholz A, Hinrichsen L, Groos S, Esk PC, Brandes G, Ungewickell EJ (2005). Effect of clathrin assembly lymphoid myeloid leukemia protein depletion on clathrin coat formation. Traffic 6, 1225–1234.
Miki K, Qu W, Goulding EH, Willis WD, Bunch DO, Strader LF, Perreault SD, Eddy EM, O'Brien DA (2004). Glyceraldehyde 3-phosphate dehydrogenase-S, a sperm-specific glycolytic enzyme, is required for sperm motility and male fertility. Proc Natl Acad Sci USA 101, 16501–16506.
Miller SE, Sahlender DA, Graham SC, Honing S, Robinson MS, Peden AA, Owen DJ (2011). The molecular basis for the endocytosis of small R-SNAREs by the clathrin adaptor CALM. Cell 147, 1118–1131.
Moreno RD, Alvarado CP (2006). The mammalian acrosome as a secretory lysosome: new and old evidence. Mol Reprod Dev 73, 1430–1434.
Moreno RD, Palomino J, Schatten G (2006). Assembly of spermatid acrosome depends on microtubule organization during mammalian spermiogenesis. Dev Biol 293, 218–227.
Mukai C, Okuno M (2004). Glycolysis plays a major role for adenosine triphosphate supplementation in mouse sperm flagellar movement. Biol Reprod 71, 540–547.
Mukai C, Travis AJ (2012). What sperm can teach us about energy production. Reprod Domest Anim 47 (Suppl 4), 164–169.
Mundy AJ, Ryder TA, Edmonds DK (1995). Asthenozoospermia and the human sperm mid-piece. Hum Reprod 10, 116–119.
Nakamura N, Rabouille C, Watson R, Nilsson T, Hui N, Slusarewicz P, Kreis TE, Warren G (1995). Characterization of a *cis*-Golgi matrix protein, GM130. J Cell Biol 131, 1715–1726.
Narisawa S, Hecht NB, Goldberg E, Boatright KM, Reed JC, Millan JL (2002). Testis-specific cytochrome c-null mice produce functional sperm but undergo early testicular atrophy. Mol Cell Biol 22, 5554–5562.
Natsume W, Tanabe K, Kon S, Yoshida N, Watanabe T, Torii T, Satake M (2006). SMAP2, a novel ARF GTPase-activating protein, interacts with clathrin and clathrin assembly protein and functions on the AP-1-positive early endosome/*trans*-Golgi network. Mol Biol Cell 17, 2592–2603.
Nonet ML, Holgado AM, Brewer F, Serpe CJ, Norbeck BA, Holleran J, Wei L, Hartwieg E, Jorgensen EM, Alfonso A (1999). UNC-11, a *Caenorhabditis elegans* AP180 homologue, regulates the size and protein composition of synaptic vesicles. Mol Biol Cell 10, 2343–2360.
Ogawa T, Arechaga JM, Avarbock MR, Brinster RL (1997). Transplantation of testis germinal cells into mouse seminiferous tubules. Int J Dev Biol 41, 111–122.
Okabe M, Ikawa M, Kominami K, Nakanishi T, Nishimune Y (1997). "Green mice" as a source of ubiquitous green cells. FEBS Lett 407, 313–319.
Paiardi C, Pasini ME, Gioria M, Berruti G (2011). Failure of acrosome formation and globozoospermia in the wobbler mouse, a Vps54 spontaneous recessive mutant. Spermatogenesis 1, 52–62.
Pierre V, Martinez G, Coutton C, Delaroche J, Yassine S, Novella C, Pernet-Gallay K, Hennebicq S, Ray PF, Arnoult C (2012). Absence of Dpy19l2, a new inner nuclear membrane protein, causes globozoospermia in mice by preventing the anchoring of the acrosome to the nucleus. Development 139, 2955–2965.
Piomboni P, Focarelli R, Stendardi A, Ferramosca A, Zara V (2012). The role of mitochondria in energy production for human sperm motility. Int J Androl 35, 109–124.
Rainey MA *et al.* (2010). The endocytic recycling regulator EHD1 is essential for spermatogenesis and male fertility in mice. BMC Dev Biol 10, 37.
Randazzo PA, Hirsch DS (2004). Arf GAPs: multifunctional proteins that regulate membrane traffic and actin remodelling. Cell Signal 16, 401–413.
Rizo J, Sudhof TC (2002). Snares and Munc18 in synaptic vesicle fusion. Nat Rev Neurosci 3, 641–653.
Roqueta-Rivera M, Abbott TL, Sivaguru M, Hess RA, Nakamura MT (2011). Deficiency in the omega-3 fatty acid pathway results in failure of acrosome biogenesis in mice. Biol Reprod 85, 721–732.
Spang A, Shiba Y, Randazzo PA (2010). Arf GAPs: gatekeepers of vesicle generation. FEBS Lett 584, 2646–2651.
Susi FR, Leblond CP, Clermont Y (1971). Changes in the Golgi apparatus during spermiogenesis in the rat. Am J Anat 130, 251–267.
Suzuki-Toyota F, Ito C, Toyama Y, Maekawa M, Yao R, Noda T, Toshimori K (2004). The coiled tail of the round-headed spermatozoa appears during epididymal passage in GOPC-deficient mice. Arch Histol Cytol 67, 361–371.
Tanabe K, Kon S, Natsume W, Torii T, Watanabe T, Satake M (2006). Involvement of a novel ADP-ribosylation factor GTPase-activating protein, SMAP, in membrane trafficking: implications in cancer cell biology. Cancer Sci 97, 801–806.
Tanabe K, Torii T, Natsume W, Braesch-Andersen S, Watanabe T, Satake M (2005). A novel GTPase-activating protein for ARF6 directly interacts with clathrin and regulates clathrin-dependent endocytosis. Mol Biol Cell 16, 1617–1628.
Wilton LJ, Temple-Smith PD, de Kretser DM (1992). Quantitative ultrastructural analysis of sperm tails reveals flagellar defects associated with persistent asthenozoospermia. Hum Reprod 7, 510–516.
Wong WF *et al.* (2010). Over-expression of Runx1 transcription factor impairs the development of thymocytes from the double-negative to double-positive stages. Immunology 130, 243–253.
Xiao N, Kam C, Shen C, Jin W, Wang J, Lee KM, Jiang L, Xia J (2009). PICK1 deficiency causes male infertility in mice by disrupting acrosome formation. J Clin Invest 119, 802–812.
Xu X (2003). Impaired meiotic DNA-damage repair and lack of crossing-over during spermatogenesis in BRCA1 full-length isoform deficient mice. Development 130, 2001–2012.
Yao R, Ito C, Natsume Y, Sugitani Y, Yamanaka H, Kuretake S, Yanagida K, Sato A, Toshimori K, Noda T (2002). Lack of acrosome formation in mice lacking a Golgi protein, GOPC. Proc Natl Acad Sci USA 99, 11211–11216.
Zhang B, Koh YH, Beckstead RB, Budnik V, Ganetzky B, Bellen HJ (1998). Synaptic vesicle size and number are regulated by a clathrin adaptor protein required for endocytosis. Neuron 21, 1465–1475.